# Mutations of Nonconserved Residues within the Calcium Channel $\alpha_1$-interaction Domain Inhibit β-Subunit Potentiation

Giovanni Gonzalez-Gutierrez,[1,2,3] Erick Miranda-Laferte,[3] David Naranjo,[1] Patricia Hidalgo,[3] and Alan Neely[1]

[1]Centro de Neurociencia de Valparaíso and [2]Programa de Doctorado en Ciencias mención Neurociencia, Universidad de Valparaíso, 2349400 Valparaíso, Chile

[3]Institut für Neurophysiologie, Medizinische Hochschule Hannover, 30625 Hannover, Germany

Voltage-dependent calcium channels consist of a pore-forming subunit ($Ca_V\alpha_1$) that includes all the molecular determinants of a voltage-gated channel, and several accessory subunits. The ancillary β-subunit ($Ca_V\beta$) is a potent activator of voltage-dependent calcium channels, but the mechanisms and structural bases of this regulation remain elusive. $Ca_V\beta$ binds reversibly to a conserved consensus sequence in $Ca_V\alpha_1$, the $\alpha_1$-interaction domain (AID), which forms an α-helix when complexed with $Ca_V\beta$. Conserved aromatic residues face to one side of the helix and strongly interact with a hydrophobic pocket on $Ca_V\beta$. Here, we studied the effect of mutating residues located opposite to the AID-$Ca_V\beta$ contact surface in $Ca_V1.2$. Substitution of AID-exposed residues by the corresponding amino acids present in other $Ca_V\alpha_1$ subunits (E462R, K465N, D469S, and Q473K) hinders $Ca_V\beta$'s ability to increase ionic-current to charge-movement ratio (I/Q) without changing the apparent affinity for $Ca_V\beta$. At the single channel level, these $Ca_V1.2$ mutants coexpressed with $Ca_V\beta_{2a}$ visit high open probability mode less frequently than wild-type channels. On the other hand, $Ca_V1.2$ carrying either a mutation in the conserved tryptophan residue (W470S, which impairs $Ca_V\beta$ binding), or a deletion of the whole AID sequence, does not exhibit $Ca_V\beta$-induced increase in I/Q. In addition, we observed a shift in the voltage dependence of activation by +12 mV in the AID-deleted channel in the absence of $Ca_V\beta$, suggesting a direct participation of these residues in the modulation of channel activation. Our results show that $Ca_V\beta$-dependent potentiation arises primarily from changes in the modal gating behavior. We envision that $Ca_V\beta$ spatially reorients AID residues that influence the channel gate. These findings provide a new framework for understanding modulation of VDCC gating by $Ca_V\beta$.

## INTRODUCTION

Influx of calcium from the extracellular medium is mainly mediated by voltage-dependent calcium channels, which are classified according to their threshold into high or low voltage of activation (Ertel et al., 2000). Channels from the high voltage of activation family are composed of at least four nonhomologous subunits: the main pore-forming subunit, $Ca_V\alpha_1$, and three auxiliary subunits, $Ca_V\alpha_2/\delta$, $Ca_V\beta$, and $Ca_V\gamma$. $Ca_V\alpha_1$ encodes all the structural elements of a functional voltage-activated calcium channel (Catterall, 2000). Among the auxiliary subunits, $Ca_V\beta$ stands out as the most potent regulator of channel function and expression (Hidalgo and Neely, 2007; Dolphin, 2003). Four $Ca_V\beta$ isoforms ($Ca_V\beta_1$ to $Ca_V\beta_4$) have been cloned from four nonallelic genes, each encoding multiple splice variants. Although all $Ca_V\beta$ isoforms potentiate currents mediated by any of the $Ca_V\alpha_1$-encoding high voltage of activation channels, they do so to a different extent (Dzhura and Neely, 2003; Luvisetto et al., 2004). This current potentiation manifests itself in an increase in the ionic-current to charge-movement ratio (I/Q) (Neely et al., 1993; Olcese et al., 1996) and in the channel's open probability (Po) (Wakamori et al., 1993; Neely et al., 1995; Costantin et al., 1998; Wakamori et al., 1999; Dzhura and Neely, 2003). $Ca_V\beta$ may also increase the number of channels present in the plasma membrane by releasing them from the endoplasmic reticulum (Bichet et al., 2000). All $Ca_V\beta$ isoforms are also capable of modulating inactivation, but only $Ca_V\beta_{2a}$ inhibits voltage-dependent inactivation whereas $Ca_V\beta_{1b}$, $Ca_V\beta_3$, and $Ca_V\beta_4$ promotes it (Olcese et al., 1994; Qin et al., 1996; Sokolov et al., 2000; Restituito et al., 2000; Hering et al., 2000). A subset of $Ca_V\beta$ isoforms participate as well in the regulation of calcium channel by G-proteins (Sandoz et al., 2004a) or protein phosphorylation (Arikkath and Campbell, 2003). This diversity in modulatory capabilities stands in contrast with the existence of a single well-defined binding site shared by all $Ca_V\alpha_1$ and $Ca_V\beta$ subunits. In $Ca_V\alpha_1$, this interaction involves a highly conserved consensus sequence, the $\alpha_1$-subunit

Correspondence to Alan Neely: alan@cnv.cl

Abbreviations used in this paper: AID, $\alpha_1$-interaction domain; GV, conductance curve; I/Q, ionic-current to charge-movement ratio; Po, open probability; $Q_{on}$, charge movement; WT, wild-type.

The online version of this article contains supplemental material.



The Rockefeller University Press $30.00
J. Gen. Physiol. Vol. 132 No. 3 383–395
www.jgp.org/cgi/doi/10.1085/jgp.200709901

interaction domain (AID), which lies within the cytoplasmic loop joining the first and second repeat of $Ca_V\alpha_1$ (Pragnell et al., 1994; Fig. 1 A). According to the crystal structure of the AID–$Ca_V\beta$ complex, AID adopts an α-helical structure with the fully conserved tyrosine and tryptophan residues lying on one face of the helix, and becoming buried in a hydrophobic pocket within $Ca_V\beta$, the so called α-binding pocket (Opatowsky et al., 2004; Van Petegem et al., 2004; Chen et al., 2004). Mutations in the AID sequence change inactivation of $Ca_V\alpha_1$ (Leroy et al., 2005; Berrou et al., 2001, 2002; Geib et al., 2002; Dafi et al., 2004), suggesting that this region interacts directly with a yet to be identified component of the channel gating machinery. Residues lying on the opposite face of the AID–$Ca_V\beta$ interaction surface (AID-exposed residues, Fig. 1 A) would be available for this interaction. Interestingly, these residues are poorly conserved among $Ca_V\alpha_1$ isoforms and may be partly responsible for isoform-specific variations. Because $Ca_V\beta$'s effect on channel activation is independent of its impact on inactivation (Olcese et al., 1994), we investigated the role of the AID motif in $Ca_V\beta$-dependent potentiation by either deleting it or replacing conserved and nonconserved amino acids within it. We chose $Ca_V1.2$ for it shows the largest shift in voltage activation by $Ca_V\beta$ (Olcese et al., 1996). In the absence of $Ca_V\beta$, mutations of AID residues (E462R, K465N, D469S, and Q473K) did not alter the voltage dependence of activation, I/Q, or single channel kinetics. In contrast, $Ca_V\beta$-induced increases in I/Q and Po were severely reduced in $Ca_V1.2$ channels bearing mutations in AID-exposed residues while the apparent binding affinity for $Ca_V\beta$ remained unchanged. These mutant channels visit high Po mode less frequently than do wild-type (WT) channels without causing obvious changes in the kinetic within each gating mode. Deletion of the complete AID sequence ($Ca_V1.2$ ΔAID) shifts the voltage dependence of activation by +12 mV, suggesting that AID residues by themselves partially display the ability to modulate activation. Collectively, these findings indicate that in $Ca_V1.2$, AID-exposed residues interact with the gating machinery controlling modal gating once they are properly oriented upon $Ca_V\beta$ binding.

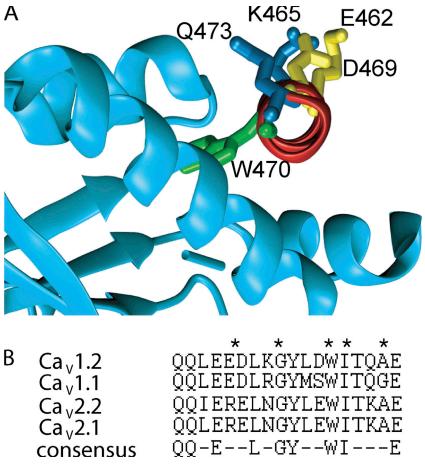


**Figure 1.** $Ca_V\beta$–AID complex and sequence alignment of AID motif. (A) Ribbon diagram of $Ca_V\beta_{2a}$–AID complex structure (Protein Data Bank ID no.: 1T0J) showing the side chain of the residues facing the hydrophilic environment and the conserved tryptophan that were mutated in this study (side chain shown in green, W470; in yellow, E462 and D469; and in blue, K465 and Q473). α-helixes encompassing the hydrophobic pocket of $Ca_V\beta2a$ are displayed in light blue, and AID α-helix is shown in red. (B) Alignment of AID sequences from several isoforms of rat $Ca_V\alpha_1$ showing positions of residues that were mutated (indicated by *).

## MATERIALS AND METHODS

### Mutagenesis

Amino acid substitutions were performed by overlapping PCR using two complementary oligonucleotides bearing the appropriate point mutation and two flanking oligonucleotides to amplify a 388-bp segment flanked by BamHI and SpeI restriction sites. The PCR product was digested with BamHI and SpeI and subcloned into pAGA-2 vector carrying the coding sequence for $Ca_V1.2$ (GenBank accession no.: X15539). The SpeI silent site was incorporated by standard PCR methods in the $Ca_V1.2$ sequence at position 497. Constructs were selected by restriction pattern and confirmed by automated DNA sequencing. $Ca_V1.2$ ΔAID was constructed by removing residues 459 to 475 (459-QLEEDLKGYLD-WITQAE-475). In all experiments, a variant of $Ca_V1.2$ bearing a deletion of 60 amino acids at the N terminus that increases expression was used (Wei et al., 1996).

### Electrophysiological Recordings and Oocyte Injection

Capped cRNAs were synthesized from Hind III-linearized templates using the MESSAGE machine (Ambion), as described previously (Hidalgo et al., 2006). Proteins and cRNAs were injected into *Xenopus* oocytes using a nanoliter injector (Nanoliter 2000; World Precision Instruments). $Ca_V\beta_{2a}$ protein was purified and handled as described by Hidalgo et al. (2006). Electrophysiological recordings were performed as in Dzhura and Neely (2003). Macroscopic currents were recorded using the cut-open oocyte voltage-clamp technique (Taglialatela et al., 1992) with a CA-1B amplifier (Dagan Corporation) 4–5 d after cRNA injection and 2–5 h after protein injection, as described in Gonzalez-Gutierrez et al. (2007). The external solution contained 10 mM $Ba^{2+}$, 96 mM n-methylglucamine, and 10 mM HEPES, and was adjusted to pH 7.0 with methanesulfonic acid. The internal solution contained 120 mM n-methylglucamine, 10 mM EGTA, and 10 mM HEPES, pH 7.0, adjusted with methanesulfonic acid. Pipettes were filled with 2 M tetramethylammonium-methanesulfonate, 50 mM NaCl, and 10 mM EGTA and showed a resistance from 0.5 to 1.2 MΩ. Current recordings were filtered at 10 kHz, and the linear components were subtracted by a P/−4 prepulse protocol. For patch-clamp recordings of single channel activity, we used an Axopatch-200B (MDS Analytical Technologies). Patch pipettes were pulled from aluminum silicate capillary (Sutter Instrument) coated with Silgard 184 (Dow Corning Corporation) and filled with a solution containing 76 mM $Ba^{2+}$, 10 mM HEPES, and 100 nM S(-)Bay K 8644 (Sigma-Aldrich), adjusted to pH 7.0 with methanesulfonic acid. Pipette resistance ranged from 3 to 8 MΩ. Oocytes were placed in the recording chamber containing 110 mM $K^+$ and 10 mM HEPES titrated to pH 7.0 with methanesulfonic acid. Calcium channels were activated by 200-ms pulses to 0 mV at

1 Hz from holding potential of −70 mV, sampled at 20 kHz, and filtered at 2 kHz. Data acquisition and analysis was performed using the pCLAMP system and software (MDS Analytical Technologies). All data are expressed as the mean ± SEM.

The presence of simultaneous openings during consecutive traces obtained after depolarization to +20 mV was the first criteria used to exclude patches containing multiple channels. From this set, the ones with no coincident openings during the next 1,000 traces using pulses to 0 mV were included in the analysis. To set a higher limit to the probability of not observing overlapping openings in a 1,000 consecutive trace, double channel patches were simulated over 5,000 traces. Channel activity was simulated as in Dzhura and Neely (2003), adjusting kinetic parameters to yield an overall Po < 0.03, as observed with E462R and K465N mutants. About 1% of the simulated traces displayed double openings. Thus, in a 1,000 traces run, the likelihood of not observing multilevel events in a two-channel patch is $(1–0.01)^{1,000} = 4.3 \times 10^{-5}$. Based on these simulations, we assumed that recordings from $Ca_V1.2$ E462R and $Ca_V1.2$ K465N channels coexpressed with $Ca_V\beta_{2a}$ did not include activity from multichannel patches. We make no assumption about the number of channels recorded using channels lacking $Ca_V\beta$; thus, in those cases we limited the analysis to burst-duration histograms.

### Online Supplemental Material

The online supplemental material includes four tables and six figures. Table S1 summarizes maximal I/Q values. Table S2 describes the parameters defining the sum of two Boltzmann distributions that best fits the normalized conductance curve (GV) for mutant and WT channels in the absence or presence of $Ca_V\beta_{2a}$, $Ca_V\beta_{1b}$, or $Ca_V\beta_{3xo}$. Table S3 includes parameters defining the exponential distribution that best fits shut, open, and burst-duration histograms for mutants and WT channels with $Ca_V\beta$. Table S4 contains the parameters defining the exponential that best fits burst histograms from individual patches of WT and E462R and K465N mutants of $Ca_V1.2$ without $Ca_V\beta_{2a}$. Fig. S1 compares ionic currents and I/Q versus voltage plot of $Ca_V1.2$ WT, $Ca_V1.2$ W470S, and $Ca_V1.2$ ΔAID in the presence or absence of $Ca_V\beta_{2a}$. Fig. S2 compares I/Q versus voltage plots for CaV1.2 WT, $Ca_V1.2$ E462R, $Ca_V1.2$ K465N with $Ca_V\beta_{1b}$, or $Ca_V\beta_{3xo}$. Fig. S3 shows single channel current versus voltage plot for $Ca_V1.2$ WT, $Ca_V1.2$ E462R, $Ca_V1.2$ D469S, and $Ca_V1.2$ Q473K coexpressed with $Ca_V\beta_{2a}$. Examples of single channel activity from $Ca_V1.2$ D469S and $Ca_V1.2$ Q473K channels in the presence of $Ca_V\beta_{2a}$ are shown in Fig. S4. Dwell-time and burst-duration histograms are plotted in Figs. S5 and S6, respectively. The online supplemental material is available at http://www.jgp.org/cgi/content/full/jgp.200709901/DC1.

## RESULTS

### Deletion of AID Yields $Ca_V\beta$-insensitive Channels and Induces a Right Shift in the Activation Curve

Mutating the conserved tryptophan residue within the AID ($Ca_V1.2$ W470S described in Hidalgo et al., 2006) or deleting the AID sequence (as in Gonzalez-Gutierrez et al. [2007]) of $Ca_V1.2$ does not affect channel expression but abolishes $Ca_V\beta$-induced increase in I/Q (Fig. S1 and Table S1, available at http://www.jgp.org/cgi/content/full/jgp.200709901/DC1). Fig. 2 B shows that there is a near perfect overlap in the activation curves of $Ca_V1.2$ W470S with $Ca_V1.2$ WT, independently of whether the mutant channel was expressed alone or together with $Ca_V\beta_{2a}$. Here, we report that in addition, the voltage dependence of activation in $Ca_V1.2$ ΔAID channels appears shifted 12 mV toward more positive potentials (Fig. 2 B and Table S2). Half-voltages ($V_{1/2}$) for both Boltzmann components describing the conductance versus voltage plot were shifted to the right by ∼10 mV, and this difference was statistically significant ($P < 0.01$; *t* test). This suggests that residues within the AID sequence participate in $Ca_V\beta$-mediated regulation of the coupling between voltage sensor and the channel gate.

### Mutations of AID-exposed Residues Inhibit $Ca_V\beta$-mediated Increase in I/Q

To further investigate the role of AID-exposed residues in channel modulation, we replaced them by the corresponding amino acids present in other $Ca_V\alpha_1$ subunits (Fig. 1) to yield $Ca_V1.2$ E462R, $Ca_V1.2$ K465N, $Ca_V1.2$ D469S, and $Ca_V1.2$ Q473K. We also tested the effect of a charge conservative mutation by replacing glutamate at position 462 by aspartate ($Ca_V1.2$ E462D). Fig. 3 A shows voltage-clamp recordings from $Ca_V1.2$ E462D, $Ca_V1.2$

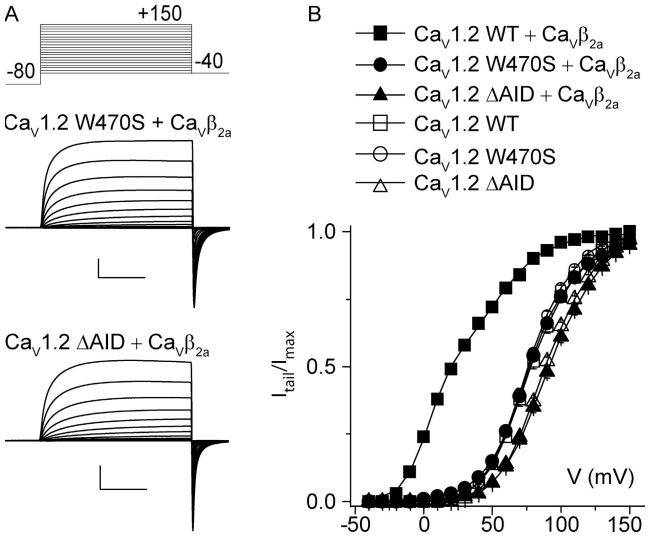


**Figure 2.** Deletion of AID sequence or replacement of the conserved tryptophan abolished modulation by $Ca_V\beta_{2a}$. (A) Superimposed macroscopic current traces from oocytes coexpressing $Ca_V\beta_{2a}$ either with $Ca_V1.2$ W470S or $Ca_V1.2$ ΔAID. Each trace was obtained during a 70-ms pulse of increasing amplitude, starting at −40 mV and ending at 150 mV in 10-mV increments. Membrane was held at −80 mV until the beginning of the pulse and returned to −40 mV for the remaining of the trace (shown at the top). Currents were sampled at 2.5 kHz until 3 ms before the end of the pulse, and then at 50 kHz. Traces were filtered at 10 kHz, and a P/−4 prepulse protocol was used to subtract linear components. Calibration bars correspond to 20 ms and 200 nA. (B) Conductance–voltage relationship (GV curve) for the different subunit combinations shown in A. The peak amplitude of the tail currents for each test voltage was normalized by the largest tail current (I/Imax) to generate the GV curves. Open and filled symbols correspond to oocytes recorded with or without $Ca_V\beta_{2a}$, respectively. The sums of two Boltzmann distributions that best described each set of data are shown as continuous lines.

E462R, and $Ca_V1.2$ K465N. In the absence of $Ca_V\beta_{2a}$, all mutants yielded I/Q versus voltage curves (Fig. 3 B) and peak values (Table S1) that were indistinguishable from $Ca_V1.2$ WT. Except for E462D, there were no apparent differences in the kinetic or voltage dependence of macroscopic currents recorded from oocytes expressing these variants in the presence of $Ca_V\beta_{2a}$. However, closer inspection revealed that inward ionic currents appeared reduced relative to the transient outward current (gating currents) for both mutants carrying a charge modification. Peak I/Q, when $Ca_V\beta_{2a}$ was coexpressed, for $Ca_V1.2$ E462R and $Ca_V1.2$ K465N were 23 and 31% of $Ca_V1.2$ WT, respectively, whereas $Ca_V1.2$ E462D in the presence or absence of $Ca_V\beta$ was nearly identical to $Ca_V1.2$ WT (Fig. 3, B and C, and Table S1). Thus, $Ca_V\beta_{2a}$ increases peak I/Q of $Ca_V1.2$ WT over 20-fold compared with sixfold and threefold for $Ca_V1.2$ E462R and $Ca_V1.2$ K465N channels, respectively. The other two mutations examined (D469S and Q473K), when coexpressed with $Ca_V\beta_{2a}$, also yield a peak I/Q smaller than $Ca_V1.2$ WT (Table S1).

To test whether these mutations hindered potentiation by other $Ca_V\beta$ isoforms, we coexpressed the isoform endogenous to *Xenopus* oocytes, $Ca_V\beta_{3xo}$ (Tareilus et al., 1997), and a rat neuronal isoform ($Ca_V\beta_{1b}$). $Ca_V\beta_{3xo}$ increased peak I/Q of WT $Ca_V1.2$ channels by ~12-fold, whereas $Ca_V\beta_{1b}$ did so by 10-fold. More importantly, $Ca_V\beta_{3xo}$ and $Ca_V\beta_{1b}$ potentiated $Ca_V1.2$ E462R and K465N channels to a lesser extend than did WT channels (Table S1 and Fig. S2, available at http://www.jgp.org/cgi/content/full/jgp.200709901/DC1). These reductions in I/Q were not accompanied by changes in the voltage dependence of activation nor in the ability of $Ca_V\beta_{2a}$ to shift the GV curves toward negative potentials (Fig. 4, A and B, and Table S2). However, the maximal conductance ($G_{max}$) normalized by charge movement ($Q_{on}$) was greatly reduced for E462R and K465N mutants in the presence of $Ca_V\beta_{2a}$ (Fig. 4 C).

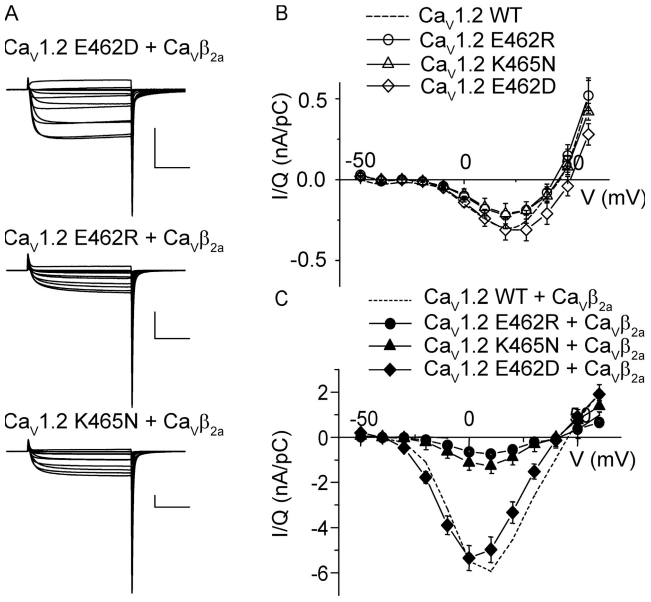


**Figure 3.** Mutations of AID-exposed residues reduce I/Q only in the presence of $Ca_V\beta_{2a}$. (A) Macroscopic currents from oocytes coexpressing $Ca_V\beta_{2a}$ with $Ca_V1.2$ E462D, $Ca_V1.2$ E462R, or $Ca_V1.2$ K465N during an IV stimulation protocol that consisted of 70-ms depolarizing pulses ranging from −50 mV to +60 mV in 10-mV increments from a holding voltage of −80 mV. Calibration bars correspond to 20 ms and 200 nA. (B) Average I/Q versus voltage plots for the indicated $Ca_V1.2$ subunits in the absence of $Ca_V\beta$. (C) Same as B but in the presence of $Ca_V\beta_{2a}$ subunit. For comparison, data from $Ca_V1.2$ WT with and without $Ca_V\beta_{2a}$ are shown as dashed lines in B and C.

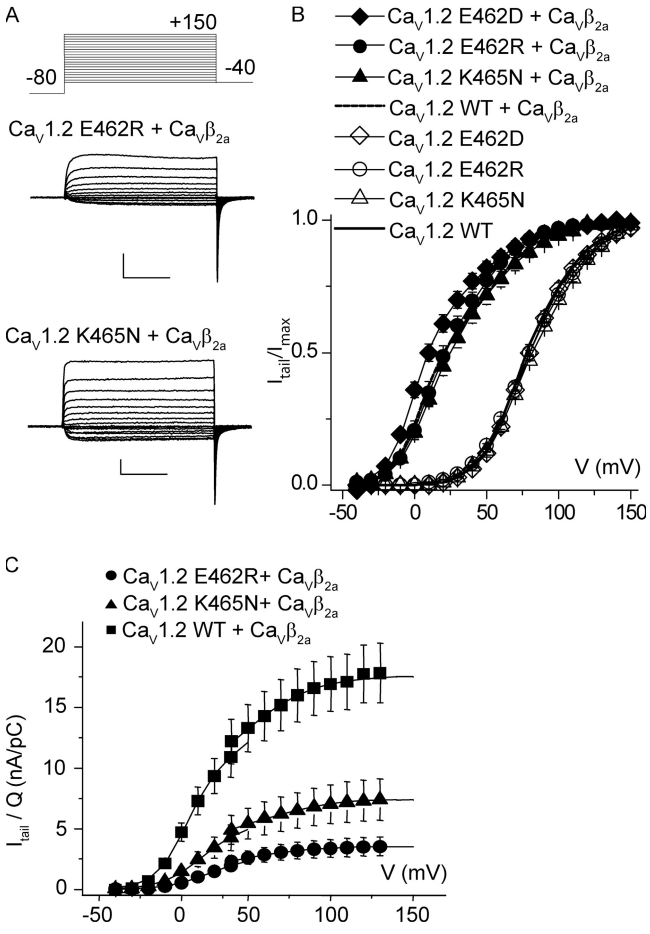


**Figure 4.** $Ca_V\beta_{2a}$ retains its ability to shift GV curves, but maximal conductances are reduced in channels bearing mutations of AID-exposed residues. (A) Macroscopic currents from oocytes coexpressing $Ca_V\beta_{2a}$ with either $Ca_V1.2$ E462R or $Ca_V1.2$ K465N during the same stimulation protocol used in Fig. 2 A (shown at the top), with calibration bars corresponding to 20 ms and 200 nA. (B) GV curves in the presence (filled symbol) or absence (open symbol) of $Ca_V\beta_{2a}$. (C) Plots of tail current amplitudes normalized by $Q_{on}$ ($I_{tail}/Q_{on}$) for $Ca_V1.2$ WT (■), $Ca_V1.2$ E462R (●), and $Ca_V1.2$ K465N (▲). $I_{tail}/Q_{on}$ (mean ± SEM) versus voltage plots were fitted to the sum of two Boltzmann distributions. The maximal $I_{tail}/Q_{on}$ was 17.8 ± 2.5 nA/pC ($n$ = 24) for $Ca_V1.2$ WT + $Ca_V\beta_{2a}$, 7.4 ± 1.74 nA/pC ($n$ = 11) for $Ca_V1.2$ K465N + $Ca_V\beta_{2a}$, and 3.5 ± 0.8 nA/pC pC ($n$ = 10) for $Ca_V1.2$ E462R + $Ca_V\beta_{2a}$.

We examined four factors that may account for this reduction in I/Q and $G_{max}$: (1) a shift in the equilibrium toward inactivated states, (2) a decrease in the fraction of channels bound to $Ca_V\beta$, (3) a decrease in unitary conductance, and (4) a reduction in the channel probability of being open.

### E462R or K465N Mutations Do Not Alter Channel Inactivation of $Ca_V1.2$ When Coexpressed with $Ca_V\beta_{2a}$

The participation of the I-II loop of $Ca_V\alpha_1$ in the regulation of voltage-dependent inactivation is well documented (Stotz et al., 2004a,b; Sandoz et al., 2004b; Berrou et al., 2001). Moreover, WT $Ca_V1.2$ coexpressed with $Ca_V\beta_{2a}$ and $Ca_V\alpha_2$ undergoes an ultraslow inactivation that develops over several seconds (Ferreira et al., 2003). Here, in the absence of $Ca_V\alpha_2$, the fraction of channels that inactivated after a 10-s depolarizing pulse did not exceed 30% over a wide range of voltages. Fig. 5 A shows the time courses of inward currents during a single 10-s pulse to 0 mV. The percentage of residual current remaining at the end of the pulse was virtually identical for WT, E462R, and K465N $Ca_V1.2$ channels (Fig. 5 B). To evaluate whether the reduction in I/Q was due to an increase in the fraction of mutant channels remaining inactive, we compared currents recorded at 0 mV after a 10-s prepulse to either −120 or −60 mV (Fig. 5 C). We were unable to detect any differences; thus, the reduction in I/Q observed in the presence of $Ca_V\beta_{2a}$ cannot be attributed to an enhancement of a slow voltage-dependent inactivation.

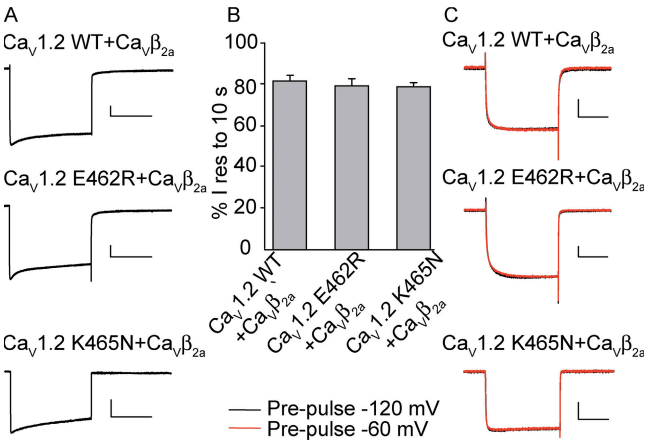


**Figure 5.** Inactivation in the presence of $Ca_V\beta_{2a}$ is not altered by E462R or K465N mutations. (A) Macroscopic currents from the indicated $Ca_V1.2$ variants during a 10-s depolarization pulse to 0 mV, with calibration bars corresponding to 5 s and 20 nA. (B) Bar plot of the percentage of currents remaining after a 10-s depolarization pulse to 0 mV for the $Ca_V1.2$ variants shown in A. Values, expressed as mean ± SEM, are 81 ± 3% ($n$ = 7) for $Ca_V1.2$ WT, 80 ± 3% ($n$ = 7) for $Ca_V1.2$ E462R, and 80 ± 2% ($n$ = 8) for $Ca_V1.2$ K465N. (C) Superimposed macroscopic currents from the same oocytes shown in A during a 200-ms pulse to 0 mV after a 10-s prepulse to either −120 mV (black) or −60 mV (red), with calibration bars corresponding to 200 ms and 20 nA.

### $Ca_V1.2$ WT, $Ca_V1.2$ E462R, and $Ca_V1.2$ K465N Channels Exhibit the Same Apparent Binding Affinity for $Ca_V\beta_{2a}$

Because $Ca_V\beta_{2a}$ shifts normalized GV curves of mutant and WT channels to the same degree, a similar fraction of channels is expected to be complexed with the auxiliary subunit and, therefore, substitutions of AID-exposed residues should not influence the affinity of $Ca_V\beta_{2a}$ for the anchoring domain. Following the same strategy used previously (Hidalgo et al. 2006), we performed dose-response experiments for each variant of $Ca_V1.2$ with purified $Ca_V\beta_{2a}$ protein and estimated the fraction of bound channels by modeling I/Q versus voltage plots (Fig. 6, A and B). In the presence of $Ca_V\beta_{2a}$, these plots differ in size and shape from the one recorded in oocytes expressing $Ca_V1.2$ variants alone. In oocytes exposed to intermediate concentrations of purified $Ca_V\beta_{2a}$, I/Q plots could be described by the weighted sum of template I/Q curves from $Ca_V1.2$ alone and from $Ca_V1.2$-expressing oocytes injected with saturating concentration of $Ca_V\beta$. The relative weight of $Ca_V1.2$-$\beta_{2a}$ template was taken as the fraction of $Ca_V\beta_{2a}$-bound channels (β2a-like). The apparent dissociation constants ($K_d$) were then calculated from the fit of β2a-like coefficients versus concentrations of purified $Ca_V\beta_{2a}$ plot to a standard Hill's equation (Fig. 6 C). The resulting values for $K_d$'s were similar for all $Ca_V1.2$ variants (0.20 µM for WT $Ca_V1.2$, 0.22 µM for $Ca_V1.2$ E462R, and 0.25 µM $Ca_V1.2$ K465N). As in Hidalgo et al. (2006), the Hill coefficient was allowed to vary freely, and best fits were obtained with values between 1.4 and 1.6. As discussed in a previous paper (Hidalgo et al., 2006), this type of experiment does not rule out a second binding site, but this seems unlikely in light of experiments showing that channel modulation is fully recapitulated by covalently linking a single $Ca_V\beta_{2b}$ to $Ca_V1.2$ (Dalton et al., 2005). On the other hand, it is possible that full equilibrium was not reached when the experiments were performed. Nevertheless, the fact that $K_d$ and Hill coefficient were virtually identical for all $Ca_V1.2$ variants strongly indicates that the fraction of $Ca_V\beta_{2a}$-bound channels was similar in all cases, and that the substituted residues indeed did not influence AID–$Ca_V\beta$ interaction. This result agrees with a recent report that $K_d$ between $Ca_V\beta$ and synthetic AID peptides derived from different $Ca_V\alpha_1$ subtypes is nearly identical (Van Petegem et al., 2008).

### AID Mutations Reduce Po of Channels Coexpressed with $Ca_V\beta$

To determine whether changes in unitary conductance contribute to the reduced I/Q in mutant channels, we measured single channel conductance in the presence of $Ca_V\beta_{2a}$ for all four mutants of AID-exposed residues ($Ca_V1.2$ E462R, $Ca_V1.2$ K465N., $Ca_V1.2$ D469S, and $Ca_V1.2$ Q473K) and found it to be ∼17 pS for all them (Fig. S3, available at http://www.jgp.org/cgi/content/full/jgp.200709901/DC1). We then compared single

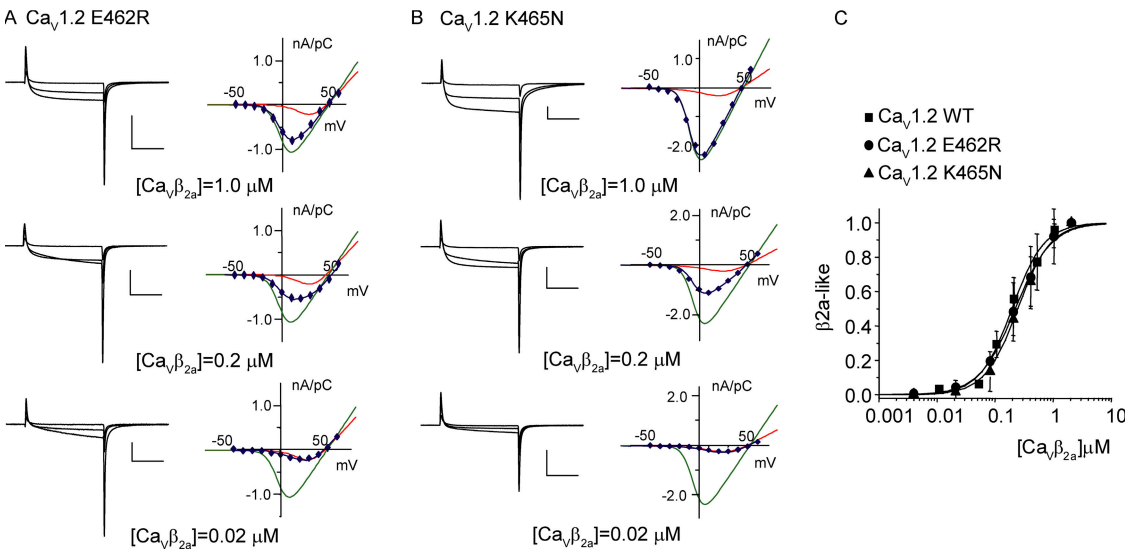


**Figure 6.** Ca$_V$1.2 E462R and Ca$_V$1.2 K465N bind to Ca$_V$β$_{2a}$ with similar apparent affinities. (A) Macroscopic current traces (right) and I/Q versus voltage from oocytes expressing Ca$_V$1.2 E462R after the injection of purified Ca$_V$β$_{2a}$ protein at the indicated concentrations. Traces correspond to superimposed responses to three 60-ms depolarizing pulses to −30 mV, 0 mV, and +30 mV from a holding voltage of −90 mV. Calibration bars correspond to 20 ms and 200 nA. Experimental I/Q values (8) were fitted to the equation (blue line):

$$I/Q = \beta 2a\_like \cdot \left[ \frac{G_{MAX}\left(V - V_{rev}\right)}{1+\exp\left(\frac{z\cdot\left(V_{1/2}-V\right)}{25.4}\right)} \right]_{+\beta 2a} + \left(1-\beta 2a\_like\right)\cdot \left[ \frac{G_{MAX}\cdot\left(V - V_{rev}\right)}{1+\exp\left(\frac{z\cdot\left(V_{1/2}-V\right)}{25.4}\right)} \right]_{-\beta 2a}.$$

Each member of the equation corresponds to templates in absence (−β*2a*) or presence (+β*2a*) of saturating concentration of Ca$_V$β$_{2a}$ protein (2.0 μM). Variables defining each template were obtained from the fit to average I/Q plot from each condition. The contribution of +β$_{2a}$ and −β$_{2a}$ templates are shown as green and red lines, respectively. (B) As A) but for Ca$_V$1.2 K465N. (C) Mean ± SE of β2a-like versus protein concentration ([Ca$_V$β$_{2a}$]) in μM. Continuous lines show the fit to a standard Hill equation:

$$\beta 2a\_like = \frac{100}{1+\left(\frac{K_d}{[Ca_V\beta_{2a}]}\right)^n}.$$

Where $K_d$ is the apparent dissociation constant and $n$ is the Hill coefficient. $n$ ranged between 1.4 and 1.6, whereas $K_d$ for WT, E462R, and K465N was 0.20, 0.22, and 0.25 μM, respectively. The number of averaged experiments ranged from three to six for every concentration and calcium channel variant.

channel activity in 1,000 traces that recorded the responses to 200-ms pulses to 0 mV repeated once a second as in Dzhura and Neely (2003). Fig. 7 A shows 20 consecutive traces with this protocol for Ca$_V$1.2 E462R and Ca$_V$1.2 K465N (data for Ca$_V$1.2 D469S and Ca$_V$1.2 Q473K is shown in Fig. S4). A decrease in the overall Po in all mutants is evident by simple inspection because of the prevalence of sweeps lacking channel openings. Channel activity in traces from K465N and E462R mutants (Fig. 7), and also from D469S and Q473K channels (Fig. S4), display long bursts. These were similar to the ones that dominated activity in Ca$_V$1.2 WT in the presence of Ca$_V$β. In contrast, in Ca$_V$1.2 W470S, channel openings are rather brief, as reported for WT calcium channel expressed in the absence of Ca$_V$β (Dzhura and Neely, 2003). The Po for each trace, estimated as the fraction of time that the channel spends in the open state, was plotted with respect to trace number to yield a typical diary plot (Fig. 7 B). As reported for WT Ca$_V$1.2 (Costantin et al., 1998; Dzhura and Neely, 2003), these plots show that channel activity is clustered and all variants retain the ability to gate in the different modes. Each mode has its own set of transition rates that determine the channel Po within a trace, which is also revealed in Po histograms using log binning (Fig. 7 C). These histograms are clearly multimodal and demonstrate that the Po among active sweeps for Ca$_V$1.2 E462R and Ca$_V$1.2 WT were distributed similarly, whereas with Ca$_V$1.2 K465N, low Po sweeps were more frequent. However, low and high Po modes appear to peak at the same values for both mutants. This stands in clear contrast with Ca$_V$1.2 W470S, which is near mono-modal; it lacks sweeps with Po > 0.1, and it is dominated by sweeps with Po around 0.05. Although the chance of including

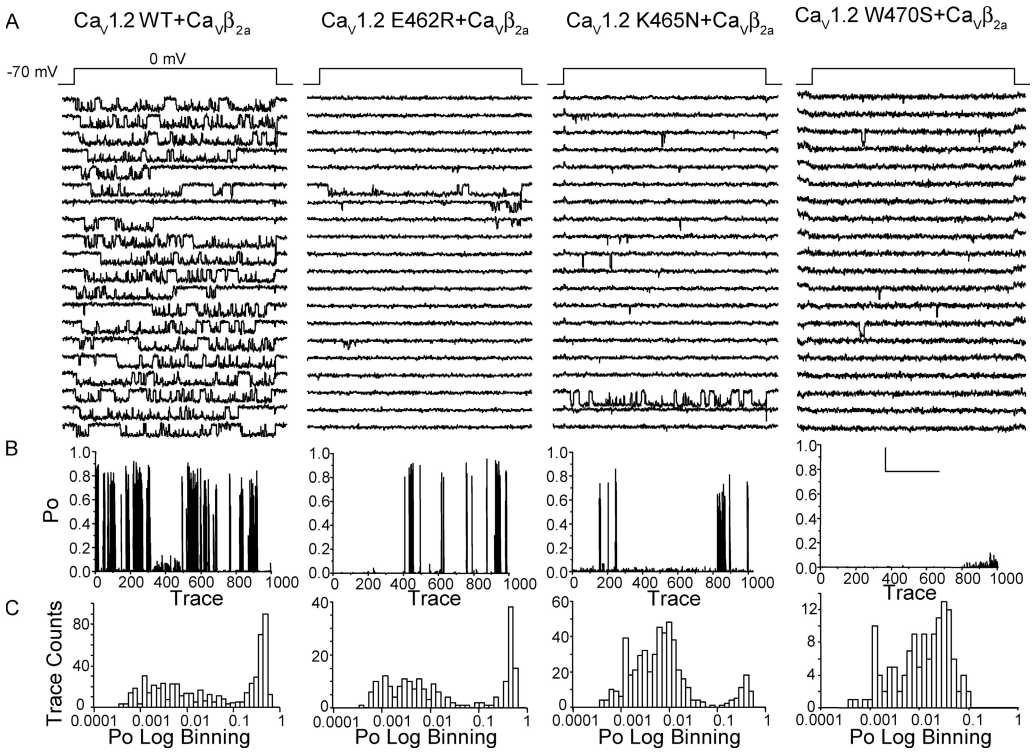


**Figure 7.** Single channel activity for different variants of $Ca_V1.2$ in the presence of $Ca_V\beta_{2a}$. (A) Representative traces from four patches containing $Ca_V1.2$ WT, $Ca_V1.2$ E462R, $Ca_V1.2$ K465N, and $Ca_V1.2$ W470S coexpressed with $Ca_V\beta_{2a}$ during 200-ms depolarizations to 0 mV repeated at 1 Hz from a holding potential of −70 mV. Calibration bar corresponds to 50 ms and 2 pA. (B) Diary plots showing the calculated Po versus trace number for $Ca_V1.2$ variant shown in A. (C) Po histograms in logarithmically binned histograms for $Ca_V1.2$ variants shown in A. Note that $Ca_V1.2$ W470S yields a mono-modal Po distribution.

traces with more than one active channel is not negligible for this mutant, the observed changes resemble those of WT $Ca_V1.2$ channels lacking $Ca_V\beta$ (Dzhura and Neely, 2003).

In Fig. 8, channel activities from several patches were compiled by normalizing the number of sweeps within each Po bin by the total number of traces in each recording. $Ca_V1.2$ W470S was excluded because of uncertainties about the number of channels in each patch. In all cases, Po histograms are bi-modals, with one mode peaking around 0.5. The low Po component is dominated by Po's between 0.001 and 0.01 in WT and E462R channels, whereas it is shifted toward slightly higher Po for K465N, D469S, and Q473K mutants (Po ≈ 0.02). However, the relative weight of each mode changed more dramatically and was quantified by calculating the fraction of null traces, non-null traces with Po ≤ 0.1, and traces with Po > 0.1 (Fig. 8 D). WT channels dwell a comparable amount of time in each mode of activity (34.3 ± 8.8, 25.6 ± 6.9, and 40.1 ± 9.2% for nulls, 0 < Po ≤ 0.1, and Po > 0.1, respectively). In contrast, all mutants rarely visit the high Po mode (6.5 ± 1.5% for $Ca_V1.2$ E462R, 4.3 ± 2.2% for $Ca_V1.2$ K465N, 8.9 ± 8.0% for $Ca_V1.2$ D469S, and 11.3 ± 6.0% for $Ca_V1.2$ Q473K). The rest of the time is spent between nulls and low Po mode, with $Ca_V1.2$ E462R visiting the low Po less frequently (16.6 ± 2.5%) compared with 40.3 ± 12.0% for $Ca_V1.2$ K465N, 37.8 ± 13.8% for $Ca_V1.2$ D469S, and 41.9 ± 10.1% for $Ca_V1.2$ Q473K. It should be noted though, that K465N, D469S, and Q473K mutants display higher patch-to-patch variability in the modal gating behavior, with low Po traces ranging from 10 to 83%. All these changes contribute to a reduction in the overall Po, which, when measured as the average fraction of time spent in the open state, ranges from 0.21 ± 0.08 for $Ca_V1.2$ WT to values ranging from 0.05 to 0.03 for mutant channels.

To visualize the impact of the decrease in Po on the macroscopic currents, mean current traces from single channel recordings were built by averaging traces during 0 mV jumps, from multiple patches for several channel variants (Fig. 9). $Ca_V1.2$ WT yields 210 fA, which compares to 29 fA for E462R and 41 fA for K465N (Fig. 9 A). This corresponds to an 86 and 81% reduction for E462R and K465N, respectively, and nearly matches the reduction in I/Q and Po described above. Single channel activity was recorded in the presence of S(-)Bay K 8644. Because the modal gating behavior may be influenced by the presence of this agonist (Lacerda and Brown, 1989), we compared I/Q versus voltage curves in the presence of 0.1 μM S(-)Bay K 8644 and 76 mM external $Ba^{2+}$ to mimic single channel recording conditions (Fig. 9 B).

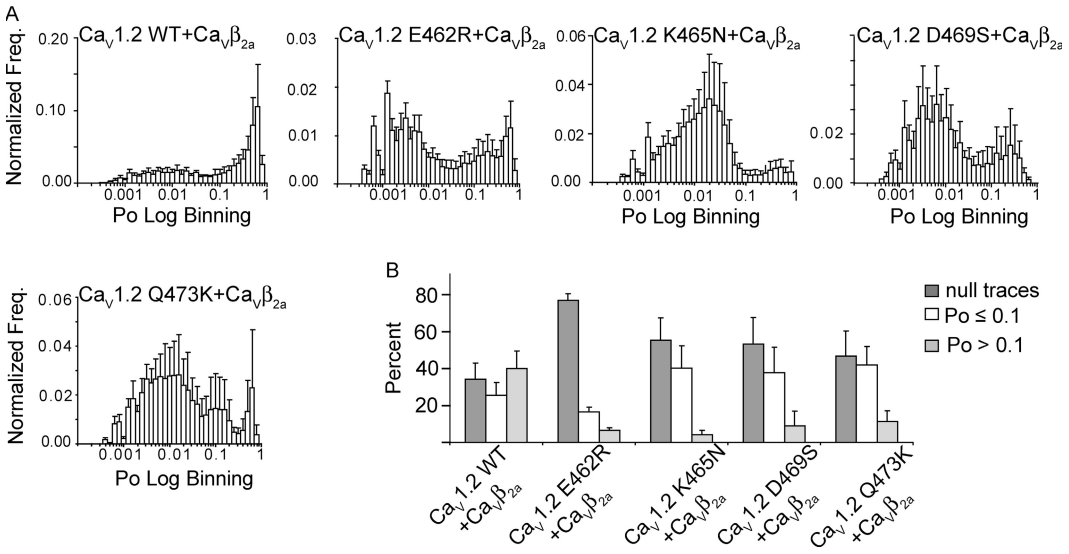


**Figure 8.** Relative frequency of Po for $Ca_V1.2$ WT, $Ca_V1.2$ E462R, $Ca_V1.2$ K465N, $Ca_V1.2$ D469S, and $Ca_V1.2$ Q473K in the presence of $Ca_V\beta_{2a}$. (A) Log-binned Po histograms compiled from several patches in the presence of $Ca_V\beta_{2a}$ for the different variant of $Ca_V1.2$ as indicated in each plot. (B) Bar plot showing percentage of null traces (dark gray), traces with Po ≤ 0.1 (white), and traces with Po > 0.1 (gray) for the different $Ca_V1.2$ variants. The percentage of traces in the different categories were similar in $Ca_V1.2$ WT (34.3 ± 8.8, 25.6 ± 6.9, and 40.1 ± 9.2% for null traces, Po ≤ 0.1, and high Po > 0.1, respectively; $n = 6$), whereas the percentage of traces with Po > 0.1 was significantly smaller ($t$ test; $P < 0.05$) for $Ca_V1.2$ E462R (6.5 ± 1.5%; $n = 7$), $Ca_V1.2$ K465N (4.3 ± 2.2%; $n = 6$), $Ca_V1.2$ D469S (8.9 ± 8.0%; $n = 4$), and $Ca_V1.2$ Q473 (11.3 ± 6.0%; $n = 4$). The fraction of low Po traces (Po ≤ 0.1) was significantly higher for $Ca_V1.2$ K465N (40.3 ± 12.0%), $Ca_V1.2$ D469S (37.8 ± 13.8%), and $Ca_V1.2$ Q473Q (41.9 ± 10.1%) than for $Ca_V1.2$ E462R (16.6 ± 2.5%). Comparing the percentage of null sweeps, only $Ca_V1.2$ E462R (78.9 ± 3.6%) is significantly higher than $Ca_V1.2$ WT (34.3 ± 8.8%). For $Ca_V1.2$ K465N, 55.4 ± 12.2% of the traces are nulls, which compares to 53.3 ± 14.4 and 46.8 ± 13.7% for $Ca_V1.2$ D469S and $Ca_V1.2$ Q473, respectively.

I/Q's for $Ca_V1.2$ E462R and $Ca_V1.2$ K465N were 77 and 63% smaller than for $Ca_V1.2$ WT, respectively, under the same recording conditions. This compares to the 87 and 79% difference in I/Q's observed in 10 mM $Ba^{2+}$ and in the absence of the calcium channel agonist, indicating that differences in Po cannot be attributed to a differential effect of S(-)Bay K 8644. Collectively, these data show that the reduction in current capacity in channels bearing a mutation in AID-exposed residues and in the presence of $Ca_V\beta_{2a}$ results from a decrease in Po associated with a decrease in the time spent in high Po mode.

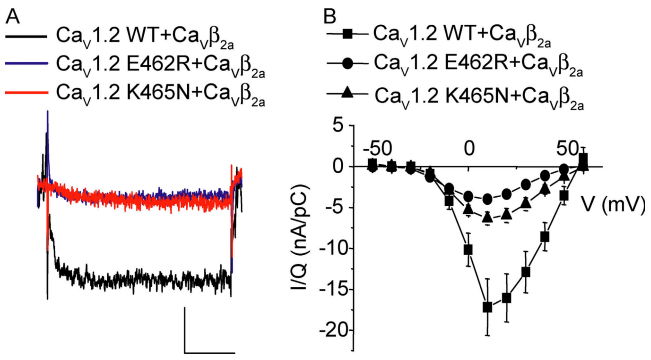


**Figure 9.** Single channel mean currents and I/Q plots from macroscopic currents from different $Ca_V1.2$ variants recorded in high $Ba^{2+}$ and S(-)Bay K8644. (A) Mean current traces for six patches containing single $Ca_V1.2$ WT/$Ca_V\beta_{2a}$ channels (black) from seven patches with $Ca_V1.2$ E462R/$Ca_V\beta_{2a}$ channels (blue), and from 6 with $Ca_V1.2$ K465N/$Ca_V\beta_{2a}$ channels (red). The number of traces averaged in each case was 4,032 for $Ca_V1.2$ WT/$Ca_V\beta_{2a}$, 7,504 for $Ca_V1.2$ E462R/$Ca_V\beta_{2a}$, and 6,104 for $Ca_V1.2$ K465N/$Ca_V\beta_{2a}$. Voltage protocol and recording condition were as described in Fig 7. Calibration bars correspond to 50 ms and 100 fA. (B) I/Q versus voltage plot for $Ca_V1.2$ WT ($n = 12$), $Ca_V1.2$ E462R ($n = 12$), and $Ca_V1.2$ K465N ($n = 13$) coexpressed with $Ca_V\beta_{2a}$ and recorded in external 76 mM $Ba^{2+}$ and 0.1 μM of S(-) Bay K 8644 as used for single channel.

### Kinetics within Gating Modes Is Similar in Channels Bearing Mutations of AID-exposed Residues and Coexpressed with $Ca_V\beta$

To evaluate if AID-exposed residues also modulate gating within each mode, we performed a standard dwell-time analysis for the different mutants. Fig. 10 shows open and shut-time histograms from the same patches shown in Fig. 7, but displayed in Sine-Sigworth coordinates. The maximum likelihood algorithm (Sigworth and Sine, 1987) was used to optimize multi-exponential probability density functions. Histograms for $Ca_V1.2$ WT and mutant channels are better described by the sum of two exponential distributions. The mean lifetime of long- and short-lived open states are indistinguishable between $Ca_V1.2$ WT and channels bearing mutations of AID-exposed residues (Table S3, available at http://www.jgp.org/cgi/content/full/jgp.200709901/DC1). In contrast, single channel activity from $Ca_V1.2$ W470S mimicked the

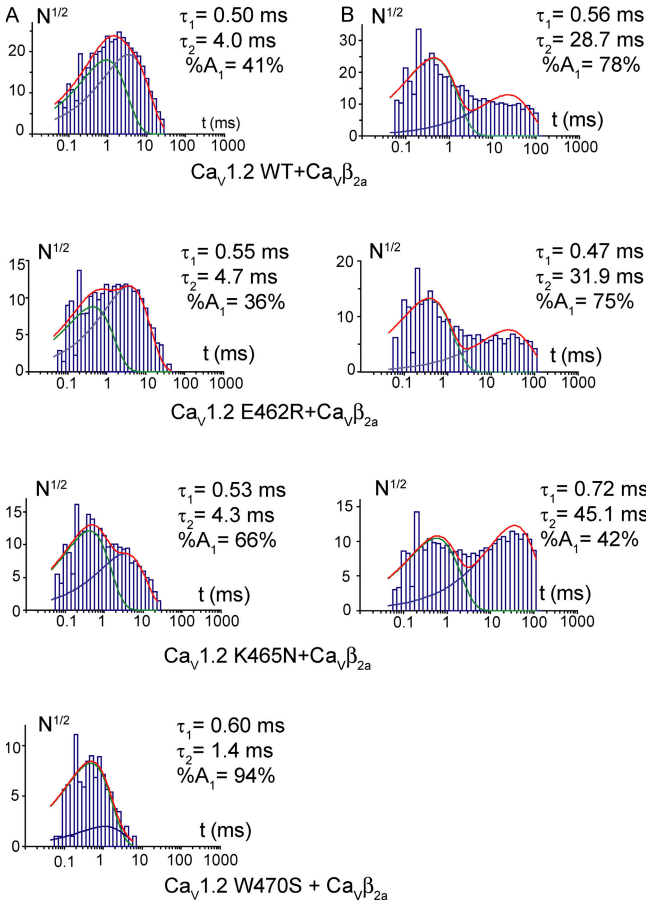


**Figure 10.** Dwell-time histograms for $Ca_V1.2$ WT, $Ca_V1.2$ E462R, $Ca_V1.2$ K465N, and $Ca_V1.2$ W470S in the presence of $Ca_V\beta_{2a}$. (A) Representative open-time histograms in Sine-Sigworth coordinates for the indicated $Ca_V1.2$ variants. The sum of the two exponential distributions that best fit the data are shown in red, and individual components are shown in blue and green. (B) Similar to A, but for shut-time histograms. The recordings used for Fig. 7 were used for the analysis shown here.

activity of WT channels recorded in the absence of $Ca_V\beta$ (Dzhura and Neely, 2003). The relative contribution of short-lived openings, typical of low Po activity, was significantly larger in mutants with 25% of the active traces being low Po ($Ca_V1.2$ K465N, $Ca_V1.2$ D469S, and $Ca_V1.2$ Q473K). This should not come as a surprise because the apparent mean open-time in low Po sweeps is shorter (Dzhura and Neely, 2003), and their contribution should be augmented in channels that visit this mode of gating more often. Differences in shut-interval histograms, meaning the lifetime and relative contribution of short and long events, were not correlated with the prevalence of the different gating mode in any obvious manner and did not help in detecting changes in the kinetic within modes.

We next compared burst-duration histograms containing all traces and described them by the sum of two exponential distributions (Fig. 11 A). In all cases, the fast component had a mean lifetime of a fraction of a millisecond, whereas longer-lived burst of openings had a mean duration around 10 ms for all variants, except $Ca_V1.2$ W470S. In this mutant, long-lived bursts averaged 4.0 ± 0.8 ms, similar to what was previously reported for WT channels lacking $Ca_V\beta$ (Dzhura and Neely, 2003). To separate bursts originating from different gating modes, histograms were built using traces with Po > 0.1 or 0 < Po ≤ 0.1. From this analysis, we can see that burst-duration histograms for Po ≤ 0.1 still required the sum of two exponential distributions for their description (Fig. 11 B), and that the time constants and relative contributions of both components were similar in all cases (Table S3). In contrast, burst-duration histograms from Po > 0.1 traces was described by a single exponential distribution with an estimated mean burst duration that ranges from 8.7 to 17.5 ms (Fig. 10 C, and Fig. S6 and Table S3, which are available at http://www.jgp.org/cgi/content/full/jgp.200709901/DC1). On average, mean burst duration for $Ca_V1.2$ WT is 11.9 ± 1.2 ms ($n = 6$), which compares to 10.9 ± 1.9 ms ($n = 7$) for $Ca_V1.2$ E462R. Although only one half of the patches displayed a reasonable number of traces with Po > 0.1, a similar value was obtained for K465N (10.9 ± 3.6 ms; $n = 3$). Similarly, mean burst durations obtained for $Ca_V1.2$ D469S and $Ca_V1.2$ Q473K were 9.1 ± 1.1 ms ($n = 4$) and 9.7 ± 3.2 ms ($n = 4$), respectively. Collectively, these results indicate that the kinetic within modes is rather insensitive to mutations of AID-exposed residues in contrast to the impact in modal gating.

### Single Channel Behavior in the Absence of $Ca_V\beta_{2a}$ Is Similar in WT $Ca_V1.2$, $Ca_V1.2$ E462R, and $Ca_V1.2$ K465N

In the absence of $Ca_V\beta$, the different $Ca_V1.2$ mutants yielded similar I/Q's (Fig. 3 B), suggesting that these AID mutations do not alter intrinsic gating of the calcium channel. As shown in Fig. 12, single channel activity appeared strikingly similar for all mutants. Unfortunately, channel activity underlying the expression of $Ca_V\alpha_1$ by itself is insufficient to rule out the presence of multiple channels; thus, long-shut intervals do not reflect a state lifetime. Consequently, only burst-duration histograms from all sweeps were compared, and two exponential distributions were required to describe them. All parameters for $Ca_V1.2$ E463R and $Ca_V1.2$ K465N turned out to be similar to those for WT channels (Table S4, available at http://www.jgp.org/cgi/content/full/jgp.200709901/DC1), indicating that the mutant phenotype is only expressed in the presence of $Ca_V\beta$. This suggests that AID-exposed residues come into place to interact with the gating machinery only when they are bound to this auxiliary subunit.

## DISCUSSION

The main conclusion of this work is that substitutions of residues on the opposite face of the AID–$Ca_V\beta$

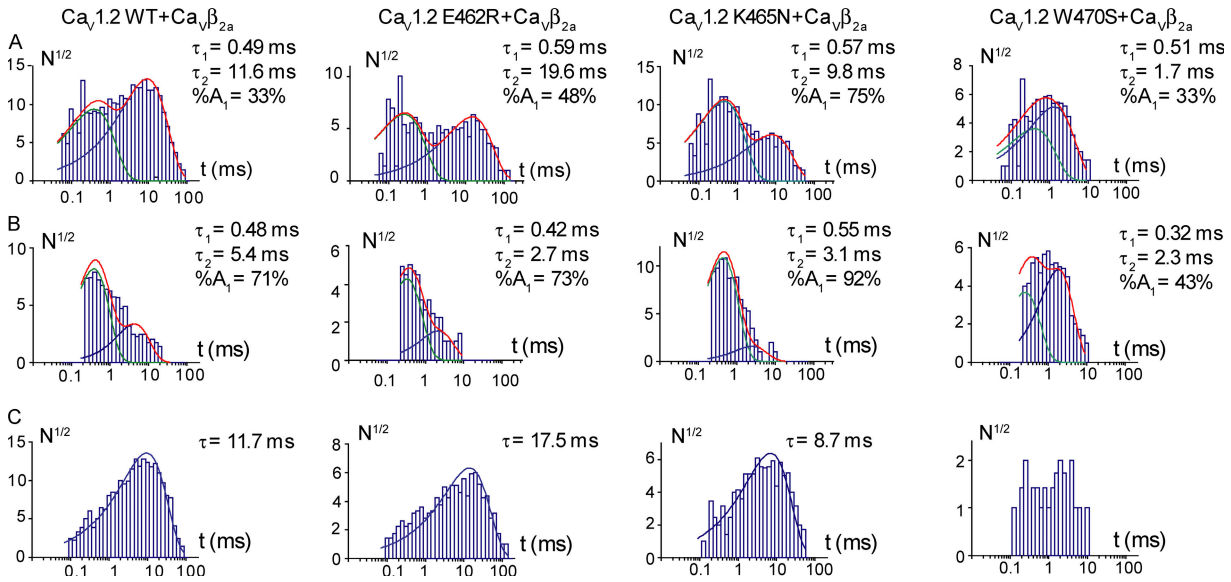


**Figure 11.** Burst-duration histograms for Ca$_V$1.2 WT, Ca$_V$1.2 E462R, Ca$_V$1.2 K465N, and Ca$_V$1.2 W470S in the presence of Ca$_V$β$_{2a}$. Openings separated by brief closings of less than 1 ms were included in the same burst. To build histograms, bursts coming from all traces were used in A, traces with Po ≤ 0.1 were chosen in B, and traces with Po > 0.1 were used in C. In A and B, the sum of two exponential distributions was necessary to describe the data (red line). Individual exponential components are shown in blue and green. A single exponential distribution was sufficient to describe burst duration histogram from traces with Po > 0.1. For W470S, an exponential fit was not attempted due to the limited number of events. The same recordings shown in Fig. 7 were used here.

interaction surface, the so-called AID-exposed residues, reduce channel current capacity only when Ca$_V$β is present. The change in the ionic-current versus voltage relationship, when normalized by Q$_{on}$, demonstrates that channel function rather than trafficking or expression is altered by these mutations. In single channel recordings,

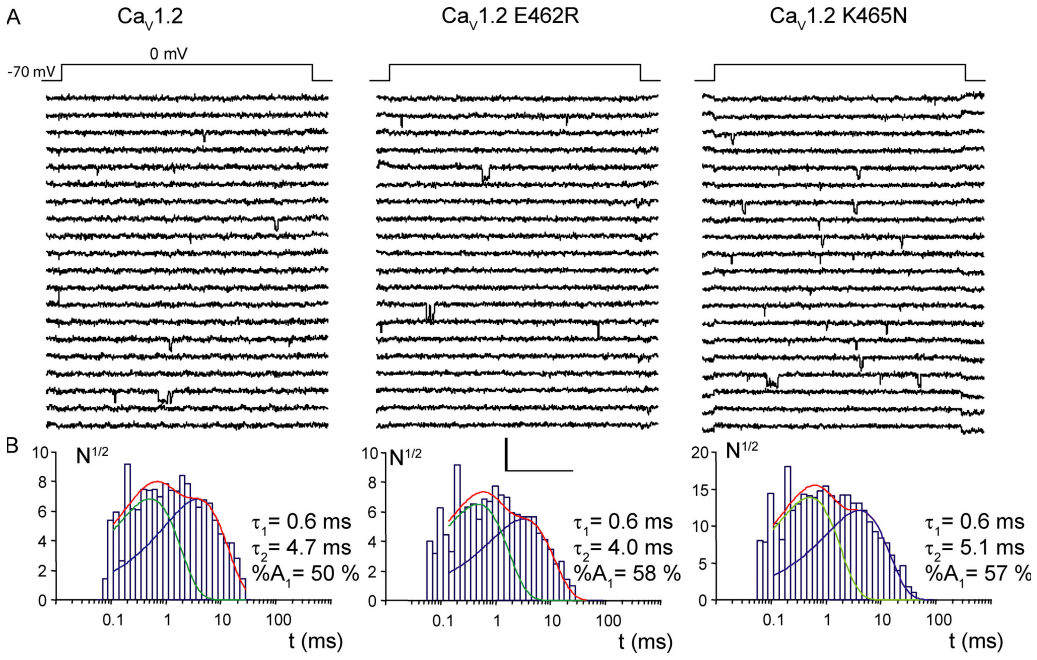


**Figure 12.** Single channel activity and burst duration histograms for Ca$_V$1.2 WT, Ca$_V$1.2 E462R, Ca$_V$1.2 K465N, and Ca$_V$1.2 W470S in the absence of Ca$_V$β$_{2a}$. (A) Representative traces of patches containing Ca$_V$1.2 WT, Ca$_V$1.2 E462R, or Ca$_V$1.2 K465N in the absence of Ca$_V$β$_{2a}$ in identical recording condition as in Fig. 7. Calibration bar corresponds to 50 ms and 2 pA. (B) Burst-duration histograms for Ca$_V$1.2 WT, E462R, and K465N in the absence of Ca$_V$β. As in Fig. 11, openings separated by brief closings of less than 1 ms were included in the same burst. All traces were used to build these histograms. A sum of two exponential distributions was necessary to describe the data.

there is dramatic reduction in the overall Po, whereas unitary conductance remains constant. As described for WT $Ca_V1.2$ (Dzhura and Neely, 2003), $Ca_V1.2$ E462R, $Ca_V1.2$ K465N., $Ca_V1.2$ D469S, and $Ca_V1.2$ Q473K present clusters of openings in at least two nonsilent modes that are manifested in Po histograms using logarithmic binning. However, the relative contribution of each nonsilent mode differs among these mutants. Whereas in $Ca_V1.2$ E462R the low Po mode is seldom visited, K465N, D469S, and Q473K mutant channels spend most of their time between low Po and silent modes. On the other hand, burst-duration histograms derived from sweeps with Po > 0.1 were similar for all mutants and WT channels, suggesting that in the presence of $Ca_V\beta$, AID-exposed residues modulate channel Po changes in modal gating rather than in the kinetic within mode.

Substitutions of the conserved tryptophan residue by serine ($Ca_V1.2$ W470S) yielded channels that behave as WT channels in the absence of $Ca_V\beta$ (Dzhura and Neely, 2003). This finding appears in discrepancy with previous results showing that $Ca_V\beta_{2a}$ modulation is spared when this conserved tryptophan residue is substituted by alanine in $Ca_V2.2$ channels (Leroy et al., 2005). Nevertheless, this tryptophan is buried in the α-binding pocket of the β-subunit (Opatowsky et al., 2004; Van Petegem et al., 2004; Chen et al., 2004) and, according to a recent comprehensive survey on the energetic of $Ca_V\alpha_1$–$Ca_V\beta$ interaction, this residue is critical for binding and modulation of function by $Ca_V\beta$ (Van Petegem et al., 2008).

There are several reports indicating that AID residues or more proximal elements of the I-II loop participate in channel inactivation (Sandoz et al., 2004b; Raybaud et al., 2007; Berrou et al., 2005; Cens et al., 2006). Furthermore, it has been reported that E462R mutant of $Ca_V1.2$ channels display an acceleration of voltage-dependent inactivation when combined to $Ca_V\alpha_2/\delta$ and $Ca_V\beta_3$ (Berrou et al., 2001; Dafi et al., 2004). If the reduced Po that we observed on E462R plus $Ca_V\beta_{2a}$ stemmed from an increase in the inactivation rate, it would be visible in prolonged pulses, which we did not observe. Moreover, the fact that this mutation appears to impair $Ca_V\beta_{2a}$-mediated increase in I/Q to a larger extend than $Ca_V\beta_{1b}$, which promotes inactivation, reinforces the idea that the effect of $Ca_V\beta$ on channel activation is independent of its impact on the rate of channel inactivation (Olcese et al., 1994).

Our data confirm that calcium channels coexpressed with $Ca_V\beta$ alternate between low Po and high Po modes (Shistik et al., 1995, Dzhura and Neely, 2003, Luvisetto et al., 2004). Because $Ca_V\alpha_1$–$Ca_V\beta$ interaction is reversible (Hidalgo et al., 2006), it appears plausible that channels switch from low to high Po upon binding to $Ca_V\beta$. In such a case, a reduction in the fraction of time spent in the high Po mode should correlate with an increase in the proportion of channels lacking $Ca_V\beta$. Here, we show that $Ca_V1.2$ mutants that seldom visit the high Po mode maintain their apparent affinities constant for $Ca_V\beta$. This is entirely in line with experiments showing that AID derived from different calcium channel subtypes share the same affinity for $Ca_V\beta$ (Van Petegem et al., 2008). To explain changes in the prevalence among different gating modes, we envision instead that $Ca_V\beta$ remains attached to the channel and positions AID-exposed residues to interact with a still unknown region of $Ca_V\alpha_1$, and that this interaction may take two possible configurations to account for low and high Po modes. In the absence of this putative interaction, channel would remain in a silent mode. Changing the side chain of some of these residues, as in K465N, D469S, and Q473K mutants, destabilizes the configuration that supports high Po, and shifts the equilibrium toward low and silent mode, whereas channel-bearing E462R mutations spend most of their time in the silent mode because the stability of both configurations is reduced. Within this new framework, β-subunit potentiation of calcium channel would arise from an increase in the proportion of channels gating in the high Po mode, and the coupling efficiency between the voltage sensor and the channel can be regulated by changing the distribution of the different gating modes.

We thank Vivian Gonzalez and John Ewer for critical review and valuable comments on this manuscript.

This work was part of G.G-G. Doctoral dissertation under a CONICYT graduate fellowship and was funded by grants from Proyecto Anillo de Ciencia y Tecnología (ACT-46) to A. Neely and the Deutsche Forschung Gemeinschaft (Grant FOR 450, TP1) to P. Hidalgo.

Olaf S. Andersen served as editor.

Submitted: 8 October 2007
Accepted: 7 August 2008

## REFERENCES

Arikkath, J., and K.P. Campbell. 2003. Auxiliary subunits: essential components of the voltage-gated calcium channel complex. *Curr. Opin. Neurobiol.* 13:298–307.

Berrou, L., G. Bernatchez, and L. Parent. 2001. Molecular determinants of inactivation within the I-II linker of alpha1E (CaV2.3) calcium channels. *Biophys. J.* 80:215–228.

Berrou, L., H. Klein, G. Bernatchez, and L. Parent. 2002. A specific tryptophan in the I-II linker is a key determinant of beta-subunit binding and modulation in Ca(V)2.3 calcium channels. *Biophys. J.* 83:1429–1442.

Berrou, L., Y. Dodier, A. Raybaud, A. Tousignant, O. Dafi, J.N. Pelletier, and L. Parent. 2005. The C-terminal residues in the alpha-interacting domain (AID) helix anchor CaV beta subunit interaction and modulation of CaV2.3 channels. *J. Biol. Chem.* 280:494–505.

Bichet, D., V. Cornet, S. Geib, E. Carlier, S. Volsen, T. Hoshi, Y. Mori, and M. De Waard. 2000. The I-II loop of the Ca2+ channel alpha1 subunit contains an endoplasmic reticulum retention signal antagonized by the beta subunit. *Neuron.* 25:177–190.

Catterall, W.A. 2000. Structure and regulation of voltage-gated Ca2+ channels. *Annu. Rev. Cell Dev. Biol.* 16:521–555.

Cens, T., M. Rousset, J.P. Leyris, P. Fesquet, and P. Charnet. 2006. Voltage- and calcium-dependent inactivation in high voltage-gated Ca(2+) channels. *Prog. Biophys. Mol. Biol.* 90:104–117.

Chen, Y.H., M.H. Li, Y. Zhang, L.L. He, Y. Yamada, A. Fitzmaurice, Y. Shen, H. Zhang, L. Tong, and J. Yang. 2004. Structural basis of the alpha1-beta subunit interaction of voltage-gated Ca2+ channels. *Nature.* 429:675–680.

Costantin, J., F. Noceti, N. Qin, X. Wei, L. Birnbaumer, and E. Stefani. 1998. Facilitation by the beta2a subunit of pore openings in cardiac Ca2+ channels. *J. Physiol.* 507:93–103.

Dafi, O., L. Berrou, Y. Dodier, A. Raybaud, R. Sauve, and L. Parent. 2004. Negatively charged residues in the N-terminal of the AID helix confer slow voltage dependent inactivation gating to CaV1.2. *Biophys. J.* 87:3181–3192.

Dalton, S., S.X. Takahashi, J. Miriyala, and H.M. Colecraft. 2005. A single CaVbeta can reconstitute both trafficking and macroscopic conductance of voltage-dependent calcium channels. *J. Physiol.* 567:757–769.

Dolphin, A.C. 2003. Beta subunits of voltage-gated calcium channels. *J. Bioenerg. Biomembr.* 35:599–620.

Dzhura, I., and A. Neely. 2003. Differential modulation of cardiac Ca2+ channel gating by beta-subunits. *Biophys. J.* 85:274–289.

Ertel, E.A., K.P. Campbell, M.M. Harpold, F. Hofmann, Y. Mori, E. Perez-Reyes, A. Schwartz, T.P. Snutch, T. Tanabe, L. Birnbaumer, et al. 2000. Nomenclature of voltage-gated calcium channels. *Neuron.* 25:533–535.

Ferreira, G., E. Rios, and N. Reyes. 2003. Two components of voltage-dependent inactivation in Ca(v)1.2 channels revealed by its gating currents. *Biophys. J.* 84:3662–3678.

Geib, S., G. Sandoz, V. Cornet, K. Mabrouk, O. Fund-Saunier, D. Bichet, M. Villaz, T. Hoshi, J.M. Sabatier, and M. De Waard. 2002. The interaction between the I-II loop and the III-IV loop of Cav2.1 contributes to voltage-dependent inactivation in a beta -dependent manner. *J. Biol. Chem.* 277:10003–10013.

Gonzalez-Gutierrez, G., E. Miranda-Laferte, A. Neely, and P. Hidalgo. 2007. The Src homology 3 domain of the beta-subunit of voltage-gated calcium channels promotes endocytosis via dynamin interaction. *J. Biol. Chem.* 282:2156–2162.

Hering, S., S. Berjukow, S. Sokolov, R. Marksteiner, R.G. Weiss, R. Kraus, and E.N. Timin. 2000. Molecular determinants of inactivation in voltage-gated Ca2+ channels. *J. Physiol.* 528(Pt 2): 237–249.

Hidalgo, P., G. Gonzalez-Gutierrez, J. Garcia-Olivares, and A. Neely. 2006. The alpha1-beta-subunit interaction that modulates calcium channel activity is reversible and requires a competent alpha-interaction domain. *J. Biol. Chem.* 281:24104–24110.

Hidalgo, P., and A. Neely. 2007. Multiplicity of protein interactions and functions of the voltage-gated calcium channel beta-subunit. *Cell Calcium.* 42:389–396.

Lacerda, A.E., and A.M. Brown. 1989. Nonmodal gating of cardiac calcium channels as revealed by dihydropyridines. *J. Gen. Physiol.* 93:1243–1273.

Leroy, J., M.W. Richards, A.J. Butcher, M. Nieto-Rostro, W.S. Pratt, A. Davies, and A.C. Dolphin. 2005. Interaction via a key tryptophan in the I-II linker of N-type calcium channels is required for beta1 but not for palmitoylated beta2, implicating an additional binding site in the regulation of channel voltage-dependent properties. *J. Neurosci.* 25:6984–6996.

Luvisetto, S., T. Fellin, M. Spagnolo, B. Hivert, P.F. Brust, M.M. Harpold, K.A. Stauderman, M.E. Williams, and D. Pietrobon. 2004. Modal gating of human CaV2.1 (P/Q-type) calcium channels: I. The slow and the fast gating modes and their modulation by beta subunits. *J. Gen. Physiol.* 124:445–461.

Neely, A., X. Wei, R. Olcese, L. Birnbaumer, and E. Stefani. 1993. Potentiation by the β subunit of the ratio of the ionic current to the charge movement in the cardiac calcium channel. *Science.* 262:575–578.

Neely, A., R. Olcese, P. Baldelli, X. Wei, L. Birnbaumer, and E. Stefani. 1995. Dual activation of the cardiac Ca2+ channel alpha 1C-subunit and its modulation by the beta-subunit. *Am. J. Physiol.* 268:C732–C740.

Olcese, R., N. Qin, T. Schneider, A. Neely, X. Wei, E. Stefani, and L. Birnbaumer. 1994. The amino terminus of a calcium channel beta subunit sets rates of channel inactivation independently of the subunit's effect on activation. *Neuron.* 13(Pt 3):1433–1438.

Olcese, R., A. Neely, N. Qin, X. Wei, L. Birnbaumer, and E. Stefani. 1996. Coupling between charge movement and pore opening in vertebrate neuronal alpha 1E calcium channels. *J. Physiol.* 497:675–686.

Opatowsky, Y., C.C. Chen, K.P. Campbell, and J.A. Hirsch. 2004. Structural analysis of the voltage-dependent calcium channel beta subunit functional core and its complex with the alpha 1 interaction domain. *Neuron.* 42:387–399.

Pragnell, M., M. De Waard, M. Mori, T. Tanabe, T.P. Snutch, and K.P. Campbell. 1994. Calcium channel β-subunit binds to a conserved motif in the I-II cytoplasmic linker of the $\alpha_1$-subunit. *Nature.* 368:67–70.

Qin, N., R. Olcese, J. Zhou, O.A. Cabello, L. Birnbaumer, and E. Stefani. 1996. Identification of a second region of the beta-subunit involved in regulation of calcium channel inactivation. *Am. J. Physiol.* 271:C1539–C1545.

Raybaud, A., E.E. Baspinar, F. Dionne, Y. Dodier, R. Sauve, and L. Parent. 2007. The role of distal S6 hydrophobic residues in the voltage-dependent gating of Cav2.3 channels. *J. Biol. Chem.* 282:27944–27952.

Restituito, S., T. Cens, C. Barrere, S. Geib, S. Galas, M. De Waard, and P. Charnet. 2000. The [beta]2a subunit is a molecular groom for the Ca2+ channel inactivation gate. *J. Neurosci.* 20:9046–9052.

Sandoz, G., I. Lopez-Gonzalez, D. Grunwald, D. Bichet, X. Altafaj, N. Weiss, M. Ronjat, A. Dupuis, and M. De Waard. 2004a. Cavbeta-subunit displacement is a key step to induce the reluctant state of P/Q calcium channels by direct G protein regulation. *Proc. Natl. Acad. Sci. USA.* 101:6267–6272.

Sandoz, G., I. Lopez-Gonzalez, S. Stamboulian, N. Weiss, C. Arnoult, and M. De Waard. 2004b. Repositioning of charged I-II loop amino acid residues within the electric field by beta subunit as a novel working hypothesis for the control of fast P/Q calcium channel inactivation. *Eur. J. Neurosci.* 19:1759–1772.

Shistik, E., T. Ivanina, T. Puri, M. Hosey, and N. Dascal. 1995. $Ca^{2+}$ current enhancement by α2/δ and β subunits in *Xenopus* oocytes: contribution of changes in channel gating and α1 protein level. *J. Physiol.* 489:55–62.

Sigworth, F.J., and S.M. Sine. 1987. Data transformations for improved display and fitting of single-channel dwell time histograms. *Biophys. J.* 52:1047–1054.

Sokolov, S., R.G. Weiss, E.N. Timin, and S. Hering. 2000. Modulation of slow inactivation in class A Ca2+ channels by beta- subunits. *J. Physiol.* 527(Pt 3):445–454.

Stotz, S.C., W. Barr, J.E. McRory, L. Chen, S.E. Jarvis, and G.W. Zamponi. 2004a. Several structural domains contribute to the regulation of N-type calcium channel inactivation by the beta 3 subunit. *J. Biol. Chem.* 279:3793–3800.

Stotz, S.C., S.E. Jarvis, and G.W. Zamponi. 2004b. Functional roles of cytoplasmic loops and pore lining transmembrane helices in the voltage-dependent inactivation of HVA calcium channels. *J. Physiol.* 554:263–273.

Taglialatela, M., L. Toro, and E. Stefani. 1992. Novel voltage clamp to record small, fast currents from ion channels expressed in *Xenopus* oocytes. *Biophys. J.* 61:78–82.

Tareilus, E., M. Roux, N. Qin, R. Olcese, J.M. Zhou, E. Stefani, and L. Birnbaumer. 1997. A *Xenopus* oocyte β subunit: evidence for a role in the assembly/expression of voltage-gated calcium channels that is separate from its role as a regulatory subunit. *Proc. Natl. Acad. Sci. USA.* 94:1703–1708.

Van Petegem, F., K.A. Clark, F.C. Chatelain, and D.L. Minor Jr. 2004. Structure of a complex between a voltage-gated calcium channel beta-subunit and an alpha-subunit domain. *Nature.* 429:671–675.

Van Petegem, F., K.E. Duderstadt, K.A. Clark, M. Wang, and D.L. Minor Jr. 2008. Alanine-scanning mutagenesis defines a conserved energetic hotspot in the CaValpha1 AID-CaVbeta interaction site that is critical for channel modulation. *Structure.* 16:280–294.

Wakamori, M., G. Mikala, A. Schwartz, and A. Yatani. 1993. Single-channel analysis of a cloned human heart L-type $Ca^{2+}$ channel $\alpha_1$ subunit and the effects of a cardiac β subunit. *Biochem. Biophys. Res. Commun.* 196:1170–1176.

Wakamori, M., G. Mikala, and Y. Mori. 1999. Auxiliary subunits operate as a molecular switch in determining gating behaviour of the unitary N-type Ca2+ channel current in Xenopus oocytes. *J. Physiol.* 517(Pt 3):659–672.

Wei, X., A. Neely, R. Olcese, W. Lang, E. Stefani, and L. Birnbaumer. 1996. Increase in Ca2+ channel expression by deletions at the amino terminus of the cardiac alpha 1C subunit. *Receptors Channels.* 4:205–215.